# Orthogonal Series Generalized Likelihood Ratio Test for Failure Detection and Isolation

Steven R. Hall*
*Massachusetts Institute of Technology, Cambridge, Massachusetts 02139*
and
Bruce K. Walker†
*University of Cincinnati, Cincinnati, Ohio 45221*

**A new failure detection and isolation (FDI) algorithm for linear dynamic systems is presented. This algorithm, the Orthogonal Series Generalized Likelihood Ratio (OSGLR) test, is based on the assumption that the failure modes of interest can be represented by truncated series expansions. This assumption leads to a failure detection algorithm with several desirable properties. First, the truncated series expansions can represent a large class of failure modes. Therefore, the test is robust to failure mode uncertainty. Second, the unknown coefficients of the series expansion enter the system equations linearly. Therefore, they may be estimated using a linear estimation scheme. This greatly reduces the amount of computation required relative to other GLR-based algorithms. Finally, in the continuous time case, the steady-state false-alarm rate can be approximated asymptotically as the detection threshold becomes large. Computer simulation results are presented for the detection of the failures of actuators and sensors of a C-130 aircraft. The results show that the OSGLR test generally performs as well as the GLR test in terms of time to detect a failure and is more robust to failure mode uncertainty. However, the OSGLR test is also somewhat more sensitive to modeling errors than the GLR test.**

## I. Introduction

As the capability for on-line data processing has grown, the interest in the problem of automated failure detection in dynamic systems has increased. Many failure detection and isolation (FDI) algorithms have been proposed. Surveys of the FDI algorithms available have been made by Willsky[1] and Walker.[2] A comprehensive review of FDI algorithms will not be given here. Instead, two particular FDI algorithms are discussed to illustrate some of the difficulties involved in the failure detection problem.

An algorithm based on the generalized likelihood ratio (GLR) test has been studied by McAulay and Denlinger,[3] Willsky and Jones,[4] and others. For the GLR test, it is hypothesized that a failure of unknown onset time $\theta$ and unknown magnitude $v$ has occurred, where the effect of this failure is an additive term in either the measurement equation or the system dynamics equation. Although the GLR test is quite powerful, it does have limitations. First, it is necessary to estimate the unknown onset time of the failure $\theta$. Because $\theta$ enters the state and measurement equations nonlinearly, this estimation process can be quite difficult. In general, it is necessary to conduct an exhaustive search over a linearly expanding range of possible values to determine the maximum likelihood estimate of $\theta$. This problem is typical of FDI tests where the onset time of the failure appears as an unknown parameter in the failure hypothesis. It has led to the use of such devices as "windowing" the range of values over which the search is conducted.

Another problem with the GLR test is that the form of the failure mode signature is assumed to be known in advance. If the signature is different than the hypothesized form, the test may fail to detect the failure or, even worse, it may detect the failure but isolate the failure to the wrong component. In general, it is desirable for an FDI test to be robust. In other words, the test should perform well regardless of the exact mode of the failure. A related problem is the development of FDI algorithms that are robust to uncertainties in the dynamic model,[5-7] which remains an open research topic. In this paper, we will confine our discussion to the problem of robustness to failure mode uncertainty.

One FDI algorithm that is robust to failure mode signature uncertainty is the detection filter of Beard[8] and Jones.[9] The detection filter is a dynamic observer with the gain matrix chosen so that a failure of any particular component causes the residuals of the observer in the absence of noise to lie in a single direction or in a plane that corresponds to the type of the failure. Unfortunately, the detection filter has a number of limitations that make it unsuitable for many applications. First, the theory is limited to time-invariant systems. Furthermore, the detection filter design process suggested by Beard[8] breaks down for many systems even though it is possible to detect and isolate failures for some of these systems. Recently, Massoumnia[10] has generalized the design procedure through the use of algebraic systems theory concepts. The resulting design procedure can be very difficult to implement in practice, however.

In this paper, a new failure detection and isolation algorithm, the Orthogonal Series Generalized Likelihood Ratio (OSGLR) test, is presented that addresses the problems just discussed. The test is robust to failure mode uncertainty, at least for actuator failures. Furthermore, the test is more computationally efficient than other GLR tests.

Simulation results are presented that illustrate the application of the algorithm to the detection of failures on a C-130 aircraft. Also, the simulation results are used to compare the OSGLR test to the GLR test of Willsky and Jones.[4] Although the results presented here are applied to the problem of detecting failures in aircraft, this paper is not intended to address all the issues associated with the restructurable control problem. For a more complete discussion of this problem, see, for example, Refs. 11-14.

Received Feb. 28, 1989; revision received June 23, 1989. 

*Finmeccanica Assistant Professor of Engineering, Department of Aeronautics and Astronautics. Member AIAA.

†Associate Professor, Department of Aerospace Engineering and Engineering Mechanics. Associate Fellow AIAA.

## II. OSGLR Test

In this section, the OSGLR test is derived. First, the dynamics of the system are described, in its failed and unfailed modes of operation. As previously discussed, the unique feature of the OSGLR test is the representation of failure modes by a series expansion. Second, the measurement process is reduced to a residual process by the use of a Kalman filter based on the nominal (i.e., unfailed) system dynamics. This reduces the failure detection problem to the problem of detection a signal of known form in the presence of additive white noise. Third, the residual process is reduced to a sufficient statistic, which contains all the information about the failure. Finally, the test for the presence of a failure is given, based on the probability density of the sufficient statistic for the failed and unfailed systems.

We are interested in detecting failures in linear dynamic systems, in both continuous time and discrete time. Only the continuous time case is considered here. (The discrete time case, which is quite similar, is given in Ref. 15.) In the normal or unfailed mode of operation ($H_0$), the state equation and measurement equation are given by

$$H_0: \frac{d\boldsymbol{x}(t)}{dt} = A(t)\boldsymbol{x}(t) + \boldsymbol{w}(t) \tag{1a}$$

$$\boldsymbol{y}(t) = C(t)\boldsymbol{x}(t) + \boldsymbol{v}(t) \tag{1b}$$

where $\boldsymbol{x}(t)$ is an $n$-dimensional state vector, $\boldsymbol{y}(t)$ is an $m$-dimensional measurement vector, $A(t)$ is the state dynamics matrix, and $C(t)$ is the measurement matrix. The terms $\boldsymbol{w}(t)$ and $\boldsymbol{v}(t)$ are zero-mean, independent, Gaussian white processes with intensities $Q(t)$ and $R(t)$, respectively. In general, the state and measurement equations can also include the effects of a known control input $\boldsymbol{u}(t)$. For the analysis that follows, these terms are omitted.

For many types of failures, the failure hypothesis ($H_1$) is represented as

$$H_1: \frac{d\boldsymbol{x}(t)}{dt} = A(t)\boldsymbol{x}(t) + \boldsymbol{w}(t) + \boldsymbol{b}(t)f(t) \tag{2a}$$

$$\boldsymbol{y}(t) = C(t)\boldsymbol{x}(t) + \boldsymbol{v}(t) + \boldsymbol{d}(t)f(t) \tag{2b}$$

where $\boldsymbol{b}(t)$ and $\boldsymbol{d}(t)$ are known vectors that represent the type of the failure and $f(t)$ is the mode shape, or simply mode, of the failure. Note that, in general, $f(t)$ may be time-varying. Because the failure mode is generally unknown a priori, it would be desirable to allow the failure mode $f(t)$ to be completely arbitrary. However, this approach does not lead to a meaningful statistical test. The approach that will be taken here is to represent the mode shape $f(t)$ by a truncated series expansion. The motivation is that if the basis functions of the expansions are sufficiently rich, then it should be possible to represent general failure modes of interest (bias jumps, ramps, stuck actuators, etc.) reasonably well with this expansion.

It is assumed that the data are observed over the interval $[t_0, t_f]$. A constraint is imposed on the form of the series expansion, namely, that it have the form

$$f(t) = \sum_{i=1}^{p} a_i(t_f)\phi_i(t_f - t) \tag{3}$$

where the $a_i$ are unknown coefficients, the $\phi_i$ are the basis functions used to represent the failure mode, and $p$ is the number of basis functions used in the series expansion. (Some considerations in the choice of basis functions are discussed in Sec. IV.) Thus, the series expansion is expressed in terms of basis functions that are defined relative to the end of the observation interval $t_f$. Equation (3) may be expressed more conveniently in vector form as

$$f(t) = \boldsymbol{\phi}^T(t_f - t)\boldsymbol{a}(t_f) \tag{4}$$

Equation (4), together with Eqs. (2a) and (2b), specifies the failure hypothesis $H_1$.

Note that the left-hand side of Eq. (4) is a function only of $t$, whereas the right-hand side is a function of both $t$ and $t_f$. This apparent contradiction may be resolved by choosing the basis functions and coefficients such that the right-hand side of Eq. (4) is invariant with respect to $t_f$. This requires that $\boldsymbol{a}(t_f)$ satisfy the differential equation

$$\frac{d\boldsymbol{a}(t_f)}{dt_f} = A_a\boldsymbol{a}(t_f) \tag{5}$$

where $A_a$ is a constant matrix. Furthermore, the vector of basis functions $\phi(\tau)$ must satisfy the differential equation

$$\frac{d\boldsymbol{\phi}(\tau)}{d\tau} = A_\phi\boldsymbol{\phi}(\tau) \tag{6}$$

where $\tau$ is the backward time index defined by

$$\tau = t_f - t \tag{7}$$

and the matrices $A_a$ and $A_\phi$ are related by

$$A_a = -A_\phi^T \tag{8}$$

Given the failure hypothesis $H_0$ and $H_1$, the first step in the formulation of the likelihood ratio is to filter the data $\boldsymbol{y}(t)$ using a Kalman filter based on the hypothesis $H_0$. The fact that the Kalman filter residual is a Gaussian white process under $H_0$ simplifies the calculation of the likelihood ratio that follows. The state estimate is propagated by the differential equation

$$\frac{d\hat{\boldsymbol{x}}(t)}{dt} = A(t)\hat{\boldsymbol{x}}(t) + K(t)\boldsymbol{\gamma}(t) \tag{9}$$

where $\hat{\boldsymbol{x}}(t)$ is the state estimate, and the residual $\boldsymbol{\gamma}(t)$ is given by

$$\boldsymbol{\gamma}(t) = \boldsymbol{y}(t) - C(t)\hat{\boldsymbol{x}}(t) \tag{10}$$

$K(t)$ is the Kalman gain matrix, defined by

$$K(t) = P(t)C^T(t)R^{-1}(t) \tag{11}$$

where $P(t)$ is the covariance of the estimation error. The covariance is propagated by the Riccati differential equation

$$\frac{dP(t)}{dt} = A(t)P(t) + P(t)A^T(t) + Q(t) - P(t)C^T(t)R^{-1}(t)C(t)P(t) \tag{12}$$

The initial conditions are that $\hat{\boldsymbol{x}}(t_0) = \boldsymbol{0}$ and $P(t_0) = P_0$, where $P_0$ is the initial covariance of the state vector, which has been assumed to have zero mean.

Due to the linearity of the state and measurement equations and of the Kalman filter, the OSGLR hypotheses can be written as

$$H_0: \boldsymbol{\gamma}(t) = \boldsymbol{\gamma}_0(t) \tag{13a}$$

$$H_1: \boldsymbol{\gamma}(t) = \boldsymbol{\gamma}_0(t) + G(t)\boldsymbol{a}(t) \tag{13b}$$

where $\boldsymbol{\gamma}_0(t)$ is a zero-mean, Gaussian white process with intensity $R(t)$. The matrix $G(t)$ represents the influence of the coefficient vector $\boldsymbol{a}(t)$ on the residual when a failure is present. The influence matrix $G(t)$ is given by[15]

$$G(t) = C(t)F(t) + \boldsymbol{d}(t)\boldsymbol{\phi}^T(0) \tag{14}$$

where $F(t)$ is the matrix that represents the influence of $\boldsymbol{a}(t)$ on the estimation error when a failure is present. The matrix $F(t)$ satisfies the differential equation[15]

$$\frac{dF(t)}{dt} = [A(t) - K(t)C(t)]F(t) + F(t)A_\phi^T + [\boldsymbol{b}(t) - K(t)\boldsymbol{d}(t)]\phi^T(0) \tag{15}$$

with the initial condition $F(t_0) = 0$.

The information in the residual process can be reduced to a sufficient statistic $\chi(t)$ that contains all the information in the residuals about the two hypotheses.[16] This statistic satisfies the differential equation

$$\frac{d\chi(t)}{dt} = A_\phi \chi(t) + G^T(t)R^{-1}(t)\gamma(t) \tag{16}$$

subject to the initial condition $\chi(t_0) = 0$.

Now, $\chi(t)$ is a Gaussian random vector, because $\gamma(t)$ is a Gaussian random process. Under $H_0$, the mean of $\chi(t)$ is the zero vector. The covariance of $\chi(t)$, $S(t)$, satisfies the differential equation

$$\frac{dS(t)}{dt} = A_\phi(t)S(t) + S(t)A_\phi^T(t) + G^T(t)R^{-1}(t)G(t) \tag{17}$$

with initial condition $S(t_0) = 0$. Under $H_1$, $\chi(t)$ has the same covariance, but its mean is given by

$$E[\chi(t)|H_1] = S(t)\boldsymbol{a}(t) \tag{18}$$

Therefore, the OSGLR hypotheses can be rewritten as

$$H_0: \chi(t_f) \sim N[0, S(t_f)] \tag{19a}$$

$$H_1: \chi(t_f) \sim N[S(t_f)\boldsymbol{a}(t_f), S(t_f)] \tag{19b}$$

The log likelihood ratio for these hypotheses is

$$\Lambda[t_f, \boldsymbol{a}(t_f)] = \boldsymbol{a}^T(t_f)\chi(t_f) - \tfrac{1}{2}\boldsymbol{a}^T(t_f)S(t_f)\boldsymbol{a}(t_f) \tag{20}$$

Because the vector of coefficients $\boldsymbol{a}(t_f)$ in Eq. (20) is unknown, an appropriate decision function is the generalized likelihood ratio, which is obtained by evaluating $\Lambda$ at the maximum likelihood estimate of $\boldsymbol{a}(t_f)$. Therefore, the decision function $\mathrm{DF}(t_f)$ is defined by

$$\mathrm{DF}(t_f) = \max_{\hat{\boldsymbol{a}}(t_f)} 2\Lambda[t_f, \hat{\boldsymbol{a}}(t_f)] = \chi^T(t_f)S^{-1}(t_f)\chi(t_f) \tag{21}$$

A failure is detected whenever $\mathrm{DF}(t_f)$ exceeds a threshold that is chosen by the user. In other words, the test is given by

$$\mathrm{DF}(t) \underset{\text{continue testing}}{\overset{\text{declare a failure}}{\gtrless}} T^2 \tag{22}$$

where $T^2$ is the detection threshold. The decision function is written here with $t$ as its time argument, rather than $t_f$, to emphasize the fact that the test is implemented as a sequential test, even though it has been derived as a test based on data from a fixed interval.

Note that the OSGLR test has a relatively simple structure. The differential equations for $\chi(t)$ and $S(t)$ are simply the Kalman filter equations for estimating $\boldsymbol{a}(t)$ in information form. The state equation for $\boldsymbol{a}(t)$ is given by Eq. (5), and the measurement equation is given by Eq. (13b).

In many respects, the OSGLR test is similar to the GLR test of Willsky and Jones.[4] The GLR test also employs a Kalman filter to estimate the unknown failure magnitude $v$. Because $v$ is a constant in the GLR formulation and because the Kalman filter is implemented in information form, the resulting estimator is simply a matched filter. However, a bank of matched filters is required for the GLR test because $v$ must be estimated for each possible time of failure $\theta$. Thus, the GLR test may be computationally burdensome, especially if the number of possible failure times (i.e., the width of the "data window") is large.

It should be noted that the OSGLR equations are intimately related to the separated-bias estimation approach of Friedland[17-19] and Caglayan.[20] In particular, the OSGLR failure hypothesis describes a system in which part of the state (the unknown coefficients) is a bias, i.e., is not driven by noise. Although Friedland treated constant biases in his work, he pointed out[17] that the extension to the case of a time-varying bias is not difficult. Tacker and Lee[21] showed that the structure of the optimal estimator for a time-varying bias is the same as that developed by Friedland for a constant bias. A later derivation of Friedland's results by Ignagni[22] derived the separated-bias equations in a manner similar to the original derivation of the OSGLR equations.[15] The major difference is that the bias estimate in our work is performed in information form, rather than Kalman filter form. In this respect, the results presented here most resemble those of Friedland,[18] who showed that the bias estimation is more readily implemented in information form. Finally, Chang and Dunn[23] recognized that the failure detection algorithm of Willsky and Jones[4] is directly related to separated-bias estimation. Of course, the OSGLR test is related for the same reasons. For a complete review of separated-bias estimation and related topics, see the review paper by Friedland.[19]

## III. False Alarm Performance of the Test

An important performance measure of any FDI algorithm is the false-alarm rate. The problem of determining the false-alarm rate of an FDI test is an example of a first-passage time problem.[24,25] First-passage time problems are generally quite difficult to solve, and analytic solutions exist only for a few special cases. For instance, an expression for the false-alarm rate has not been derived for the GLR test. For the OSGLR test proposed in this paper, however, an asymptotic expression can be found for the steady-state false-alarm rate as the test threshold becomes large. The details of the derivation of this asymptotic expression can be found in Ref. 15. The result is

$$\lambda = \frac{-\mathrm{tr}[A_\phi](T^2/2)^{p/2}}{\Gamma(p/2)(p/2)} e^{-T^2/2}\left[1 - \frac{p}{T^2} + O\left(\frac{1}{T^4}\right)\right], \quad T \to \infty \tag{23}$$

where $\Gamma(\cdot)$ denotes the gamma function and $p$ denotes the number of terms in the series representation of the failure mode.

Although this expression is applicable only for large values of $T$, the threshold is often chosen to be a large value in order to minimize the frequency at which false alarms occur. Furthermore, for the case where $p = 1$, the asymptotic expression for the false-alarm rate can be checked against the exact solution obtained by numerical methods. For thresholds in the vicinity of $T = 4$ (where $\chi(t)$ must lie at least four standard deviations away from the mean value under unfailed conditions to indicate the presence of a failure), the asymptotic expression is accurate to within 1% error. The accuracy improves as the threshold becomes larger. This level of accuracy in predicting the false-alarm rate of the OSGLR test is considered adequate for most practical purposes, and it is remarkable in light of the absence of false-alarm rate expressions for essentially any other failure detection test that is not based on fixed lengths of data (including the GLR).

## IV. Implementation Considerations

The OSGLR failure hypothesis ($H_1$) is based on the heuristic argument that most failure modes can be adequately approximated by a truncated series expansion. In this section,

we briefly discuss the implications of this assumption and how it affects the choice of basis functions.

Consider the effect of a failure on the residual $\gamma(t)$. If the failure mode can be exactly represented by the series expansion (3), then the residual can be represented as in Eq. (13b). However, for a general failure mode, the residual will have the form

$$H_1: \gamma(t) = \gamma_0(t) + \boldsymbol{m}(t) \tag{24}$$

where $\boldsymbol{m}(t)$ is the mean in the residual due to the failure. When the $\chi(t_f)$ is formed from the residual, it will be a Gaussian random variable with mean value $\bar{\chi}(t_f)$ [which will depend on $\boldsymbol{m}(t)$] and covariance $S(t_f)$. Therefore, the decision function $\mathrm{DF}(t_f)$ will be a noncentral chi-squared random variable with noncentrality parameter

$$\delta^2(t_f) = \bar{\chi}(t_f) S^{-1}(t_f) \bar{\chi}(t_f) \tag{25}$$

The noncentrality parameter may be interpreted as the squared magnitude of the projection of the mean in the residual, $\boldsymbol{m}(t)$, onto the space of possible failure signatures generated by the OSGLR failure hypothesis $H_1$. As such, the noncentrality parameter is bounded by

$$\delta^2(t_f) \leq d^2(t_f) \tag{26}$$

where $d^2(t_f)$ is the signal-to-noise ratio of the failure signature $\boldsymbol{m}(t)$ over the interval $[t_0, t_f]$. Equation (26) is satisfied with equality if and only if $\boldsymbol{m}(t)$ can be expressed exactly as

$$\boldsymbol{m}(t) = G(t, t_f)\boldsymbol{a}(t_f) \tag{27}$$

Of course, we want the noncentrality parameter to be as large as possible, so that the failure will be easily detected and not confused with the failure of other components. Thus, when we require that the failure modes be approximated well by the truncated series expansion, we mean that $\delta^2(t_f)$ should be near $d^2(t_f)$ for the failure modes of interest.

If the basis functions used in the series expansion form a complete basis, $\delta^2(t_f)$ can be made arbitrarily close to $d^2(t_f)$ by choosing $p$ sufficiently large. However, $p$ cannot be made arbitarily large for two practical reasons. First, increasing $p$ increases the false-alarm rate for a given threshold. [See Eq. (23).] Second, increasing the number of basis functions increases the amount of computation required to perform the OSGLR test. Therefore, $p$ should be just large enough to satisfy the requirement that $\delta^2 \cong d^2$.

At this point, two observations are in order. The first is that because the failure signature is affected by both the plant and the Kalman filter, the number of basis functions needed to adequately represent a given failure model depends not only on the failure mode, but also on the system. In particular, actuator failures are more easily represented by the OSGLR failure hypothesis than sensor failures. The reason for this is the following: The transfer function from an actuator input to the Kalman filter residual is generally low pass in nature. Roughly speaking, the truncated terms of the series expansion are high-frequency terms. Hence, the energy represented by the OSGLR failure hypothesis $[\delta^2(t_f)]$ closely approximates the energy in the failure signature $[d^2(t_f)]$. This idea is very much like the filter hypothesis of describing function theory.[26]

On the other hand, the transfer function from a sensor to the Kalman filter residuals is generally high pass in nature. As a result, the high-frequency content of the failure mode is accentuated. Therefore, it may be quite difficult to adequately represent the failure mode of a sensor using the OSGLR failure hypothesis. Note that this problem is not unique to the OSGLR test. Any test, including the GLR test, that is based on Kalman filter residuals will be sensitive to high-frequency errors in the modeling of the failure mode of a sensor.

## V. Simulation Results

To demonstrate the use of the OSGLR test, a computer simulation of a C-130 aircraft was modified to allow the introduction of failures of flight control surface actuators. The nonlinear simulation describes the dynamics of a C-130 aircraft using six-degree-of-freedom equations of motion. The nominal operating point used in this study corresponds to cruising flight at an altitude of 1000 ft, with an airspeed of 150 kt. The aerodynamic forces and moments are described by one-, two-, and three-dimensional lookup tables. Actuator dynamics are also incorporated into the simulation, as is a flight control system with an autopilot. The surfaces available for control of the aircraft are the elevator, ailerons, rudder, and flaps (Table 1). The simulation allows for independent motion of the left and right ailerons and left and right flaps so that failures of these surfaces may be simulated.

The measurements are available (or sampled) at a rate of 50 Hz. The sensor noise is assumed to consist of independent, zero-mean Gaussian sequences, with standard deviations as given in Table 2. (The standard deviation of the rate-of-climb measurement is probably too low to be realistic. However, the results presented here do not seem to be sensitive to this sensor.)

In addition, turbulence was modeled in the simulation, since turbulence directly affects the ability to detect failures. The Dryden turbulence model[27] was used, with length scales

$$L_w = 1000 \text{ ft}$$

$$L_u = L_v = 1452 \text{ ft}$$

and

$$\sigma_w = 6.5 \text{ ft/s}$$

$$\sigma_u = \sigma_v = 7.83 \text{ ft/s} \tag{28}$$

These turbulence levels correspond to the maximum levels of clear air turbulence expected at 1000 ft, and thus represent the worst-case process noise.

**Table 1 Aircraft control surfaces**

| Control surface | Symbol | Detection decision function subscript[a] |
|---|---|---|
| Elevator, deg | $\delta_E$ | 1 |
| Right aileron, deg | $\delta_{AR}$ | 2 |
| Left aileron, deg | $\delta_{AL}$ | 3 |
| Rudder, deg | $\delta_R$ | 4 |
| Right flap, % | $\delta_{FR}$ | 5 |
| Left flap, % | $\delta_{LR}$ | 6 |

[a]Designates the detection decision function associated with each control surface.

**Table 2 Aircraft measurements**

| Measured variable | Standard deviation | Detection decision function subscript[a] |
|---|---|---|
| Airspeed, ft/s | 11.0 | 7 |
| Lateral acceleration, ft/s$^2$ | 0.984 | 8 |
| Normal acceleration, ft/s$^2$ | 0.984 | 9 |
| Roll rate, rad/s | 0.0024 | 10 |
| Pitch rate, rad/s | 0.0007 | 11 |
| Yaw rate, rad/s | 0.0007 | 12 |
| Bank angle, rad | 0.01 | 13 |
| Elevation angle, rad | 0.01 | 14 |
| Heading, rad | 0.01 | 15 |
| Rate of climb, ft/s | 0.25 | 16 |
| Barometric altitude, ft | 10.0 | 17 |

[a]Designates the detection decision function associated with each sensor.

The OSGLR test was implemented in discrete time. For each failure hypothesis, six basis functions were used in the truncated series expansion. The basis functions are the discrete-time equivalent of the Laguerre functions,[28] with time constant $\tau = 3$ s. That is, the basis functions are obtained by orthonormalizing the (discrete-time) functions

$$\phi_i(k) = k^{i-1}z^k, \qquad i = 1, 2,...,6 \tag{29}$$

where

$$z = e^{-\Delta t/\tau}, \qquad \Delta t = 0.02 \text{ s} \tag{30}$$

The Laguerre functions are a convenient choice for basis functions because they satisfy the invariance condition given in Eq. (6). Furthermore, the Laguerre functions form a complete basis, so that any failure mode may be represented by a Laguerre series of sufficient length. Of course, the series is truncated here at six terms, so that some representation error will occur. Nevertheless, the first six Laguerre functions can represent more than 90% of the energy in a discontinuous step failure for a wide range of time constants. Furthermore, much of the energy in the representation error is confined to high frequencies and therefore is filtered out by the Kalman filter. The representation of the failure signature in the residual by six Laguerre functions is therefore considered adequate. The time constant $\tau = 3$ s allows accurate representation of failure signatures over a range of times from a fraction of a second to about 30 s, which suffices for the present problem. It should be noted that the results were found to be insensitive to the choice of time constant.

As a basis for comparison, a discrete time GLR test was also implemented. The assumed failure mode of each GLR failure hypothesis is a step function (or bias) of unknown magnitude occurring at time $\theta$. This failure hypothesis is commonly assumed in failure detection. To limit the computation time required for the GLR test, the failure onset time $\theta$ is assumed to be constrained to the data window $t - t_w \le \theta \le t$, where $t_w$ is the length of the window. The results presented in this paper are for a 2 s (100 sample) data window. In contrast, a failure onset time is not included explicitly in the OSGLR failure hypothesis; therefore no data window is required for it.

The simulation results can be divided into two categories: those based on the linearized models and those based on the full nonlinear simulation. For the most part, the simulation results presented are based on the linearized models. The reasons for this are twofold. First, the linear simulations demonstrate the characteristics of the OSGLR test unobscured by nonlinear effects. Second, the linear simulation requires considerably less computation than the nonlinear simulation. Therefore, linear models are used to demonstrate the important features of the OSGLR test. The nonlinear simulation is used to show the effects of nonlinearities, and to generate test cases that are not easily generated using the linear simulation.

To determine the performance of the OSGLR and GLR algorithms, a detection threshold must be set for each. Because no performance specifications have been given, the selection of the threshold is somewhat arbitrary. We set the OSGLR threshold so that the resulting false alarm rate of each OSGLR detector is $10^{-4}$/h or less. Therefore,

$$T^2 = 56.86 \tag{31}$$

As noted earlier, the false-alarm rate is very sensitive to the selection of the threshold. As a result, the threshold is *not* very sensitive to the specification of the false-alarm rate. For example, if we require that the false-alarm rate be decreased to $10^{-6}$/h, then the threshold must be increased to only $T^2 = 67.10$. Thus, the results presented here will not be sensitive to the exact value of the false-alarm rate specification.

It is somewhat more difficult to determine the threshold for the GLR test. To compare the GLR and OSGLR tests on a fair basis, we should select the threshold for the GLR test so that each GLR detector has the same false-alarm rate as the OSGLR detectors. Unfortunately, no analytic expression for the false-alarm rate of the GLR test exists. The false-alarm rate could be determined in principal by Monte-Carlo simulation. However, the amount of simulation that would be required would be enormous, because of the very small rate at which false alarms occur. Therefore, we simply set the GLR detection threshold to the same value as the OSGLR detection threshold.

Simulation results are presented here for the following five cases: 1) elevator bias failure (linear simulation); 2) aileron bias failure (linear simulation); 3) nonlinear simulation with no failure; 4) stuck elevator (nonlinear simulation); and 5) yaw rate gyro failure (linear simulation). The first two cases illustrate the behavior of the algorithms in the absence of modeling errors. The second case is a more difficult case than the first, since it is generally difficult to distinguish among failures of the ailerons or flaps. The third case illustrates the sensitivity of the algorithms to modeling errors. The fourth case illustrates the behavior of the two algorithms in the presence of a failure mode not hypothesized by the GLR test. Finally, the fifth case shows the difficulties encountered when using the OSGLR test for sensor failures.

**Elevator Bias Failure**

In this case, a $-1$ deg bias of the elevator was simulated using the linear simulation. The failure occurred at time $t = 10$ s of a 50 s simulation.

Figure 1 shows the OSGLR detection decision functions for the six control surfaces. The decision functions generally have the characteristics that we expect. Immediately following the onset of the failure, the decision function corresponding to the elevator, $DF_1$, increases rapidly, indicating a failure of the elevator. To a lesser extent, the other decision functions increase as well, although they are always much less than $DF_1$. For the detection threshold selected, detection occurs at $t = 10.22$ s, 0.22 s after the onset of the failure.

Note that in this case, the decision function of the failed surface (i.e., $DF_1$) is much larger than the decision functions corresponding to the other surfaces. Thus, there is little doubt that the failure can be easily isolated to the correct surface.

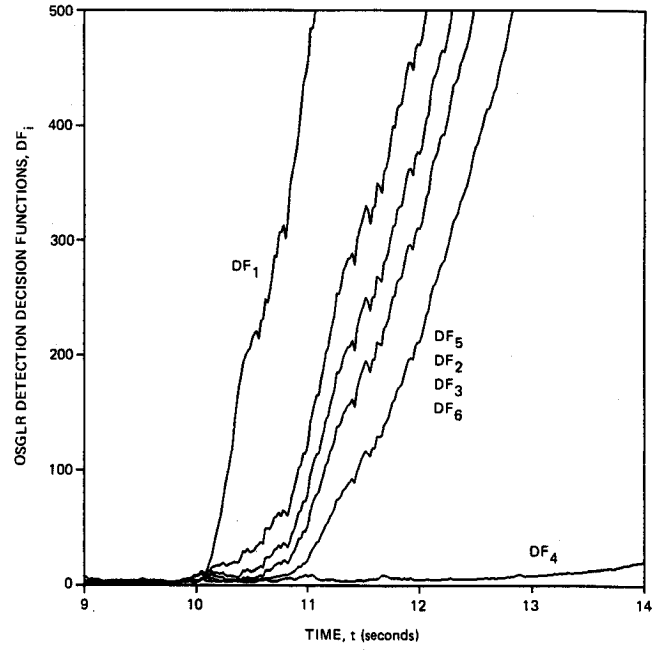


**Fig. 1 OSGLR detection decision functions for the linear simulation with a $-1$ deg bias failure of the elevator at time $t = 10$ s.**

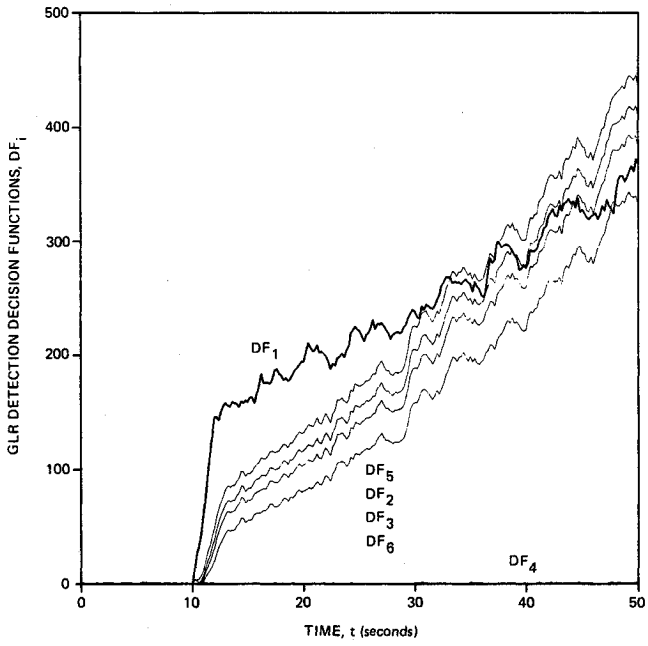


**Fig. 2 GLR detection decision functions for the linear simulation with a $-1$ deg bias failure of the elevator at time $t = 10$ s. A 2 s (100 sample) data window was used.**

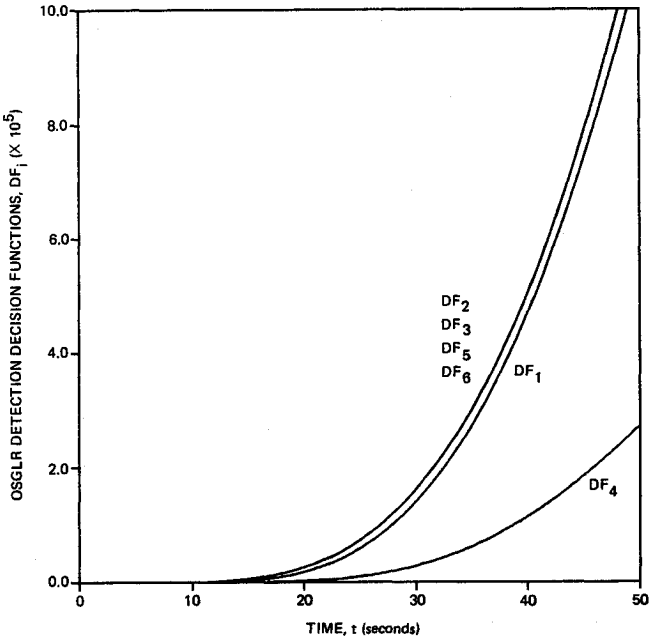


**Fig. 3 OSGLR detection decision functions for the linear simulation with a 1 deg bias failure of the right aileron at time $t = 10$ s.**

Figure 2 shows the GLR detection decision functions for the same simulation. For the 2 s period immediately following the failure, the GLR detection functions closely resemble the OSGLR decision functions. The elevator decision function increases rapidly, crossing the detection threshold at $t = 10.12$ s.

It is not surprising that the GLR detection time is less than that of the OSGLR test, because the GLR hypotheses can represent the failure mode exactly, whereas the OSGLR hypotheses can only approximate the failure mode. Also, the time scale of the basis functions is $\tau = 3$ s, which is considerably longer than the time required to detect the failure. If the time scale is reduced to $\tau = 0.5$ s, then the detection time for the OSGLR test is the same as for the GLR test. However, it was felt that the longer time scale was desirable to allow for failures that take longer to detect. Furthermore, the detection time of 0.22 s is probably acceptable.

Despite the good performance of the GLR test, the algorithm does display some undesirable characteristics. Note that at $t = 12$ s, the decision functions suddenly level off. This is due, of course, to the finite data window of the GLR test. The GLR algorithm accumulates data for only the length of the data window, which is 2 s long in this case. After that time, information about the failure is discarded.

Furthermore, note that $DF_5$ exceeds $DF_1$ after $t = 33.2$ s. Had the threshold been larger, or the failure been smaller, the GLR test could have isolated the failure to the wrong component, namely, the right flap. The reason for this behavior is again related to the data window. After $t = 12$ s, the actual failure (a step failure at $t = 10$ s) is not one of the failures considered by the GLR test. Therefore, the behavior of the algorithm is unpredictable after $t = 12$ s.

The OSGLR test does not have the undesired characteristics of the GLR test previously discussed. As discussed earlier, the OSGLR hypotheses can represent the step failure, at least approximately, over a time period as short as a fraction of a second to as long as 30 s (for the basis functions chosen). Over this time period, the OSGLR test continues to accumulate information about the failure. As a result, the OSGLR test does not display the characteristics of the GLR test which are associated with its relatively short data window. Over time periods longer than 30 s, the behavior of the OSGLR algorithm will also be unpredictable.

**Right Aileron Bias Failure**

In this case, the linear simulation was used to simulate a 1 deg bias failure of the right aileron. The failure occurred at time $t = 10$ s of a 50 s simulation.

Figure 3 shows the OSGLR detection decision functions for this simulation. Immediately following the failure, the four decision functions corresponding to the wing control surfaces ($DF_2$, $DF_3$, $DF_5$, and $DF_6$) begin to rise steadily. To the scale of the plot, these four decision functions cannot be distinguished. The elevator decision function ($DF_1$) also rises steadily following the failure. On the plot, $DF_1$ appears to be close to the four decision functions of the ailerons and flaps. On an absolute scale, however, this difference is large. Finally, the rudder decision function ($DF_4$) also increases somewhat, although not nearly so much as the other five decision functions. For the detection threshold given, the detection occurs 0.56 s after the onset of failure.

The reason that the four decision functions are nearly equal is easily explained. The primary effect of the deflection of any single wing control surface (aileron or flap) is to produce a rolling moment. To a lesser extent, lift is also produced. Since the failure of any of these surfaces will produce a similar effect, it is difficult to distinguish among them. It is only the differences in failure signatures of different components that allow failures to be isolated to a single component.

To determine which of the four detection decision functions of the wing control surfaces is largest following failure, (some of) the OSGLR isolation decision functions are plotted in Fig. 4. The isolation decision function $DF_{i,j}$ is given by

$$DF_{i,j} = DF_i - DF_j \tag{32}$$

Shown in the figure are $DF_{2,3}$, $DF_{2,5}$, and $DF_{2,6}$. Following the failure, all three of these isolation decision functions are positive, correctly indicating that the right aileron ($i = 2$) is the surface that has failed. Also, except for a brief period immediately following the failure,

$$DF_{2,6} > DF_{2,5} > DF_{2,3} \tag{33}$$

These results make sense in light of the previous discussion. That is, it is relatively easy to distinguish between failures of the right aileron (as indicated by $DF_2$) from those of the elevator ($DF_2$) or rudder ($DF_4$), but progressively more

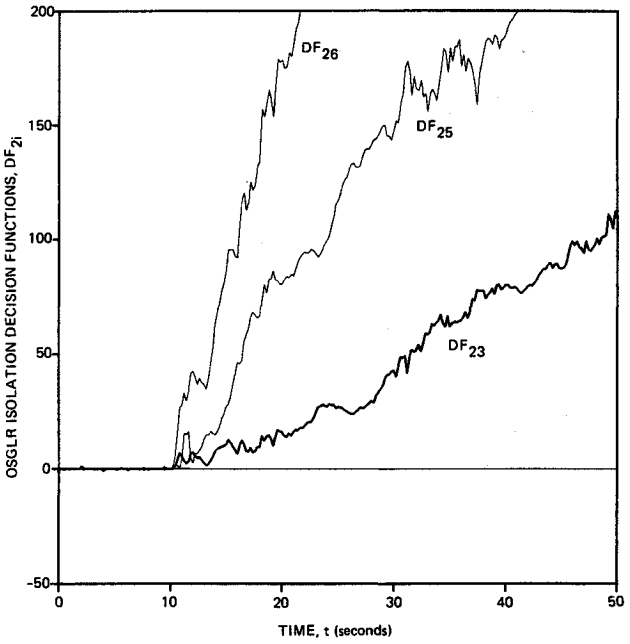


**Fig. 4 OSGLR isolation decision functions for the linear simulation with a 1 deg bias failure of right aileron at time $t = 10$ s.**

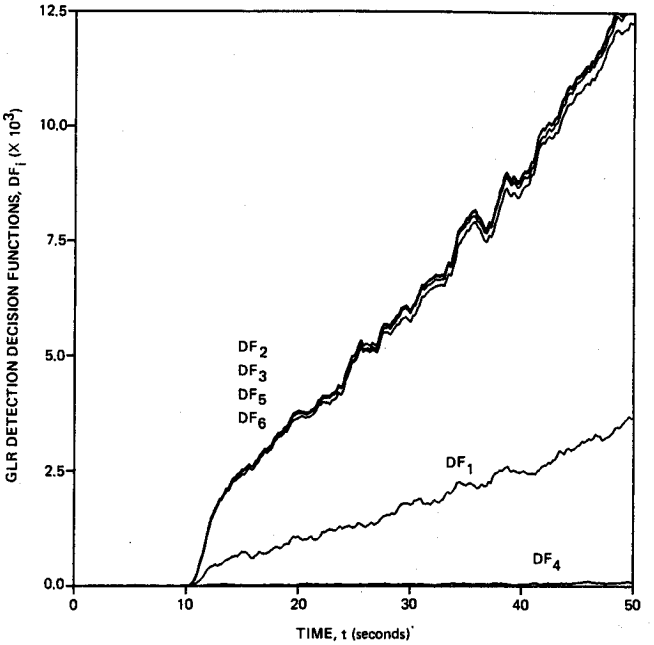


**Fig. 5 GLR detection decision functions for the linear simulation with a 1 deg bias failure of the right aileron at time $t = 10$ s.**

difficult to distinguish a right aileron failure from the failure of the left flap ($DF_6$), the right flap ($DF_5$), and the left aileron ($DF_3$).

Note that because the failure of the right aileron is barely distinguishable from failures of the other three wing control surfaces, it would be wise to use an isolated threshold for this system to prevent incorrect isolations. That is, a failure would not be isolated to a specific actuator $i$ until $DF_{i,j}$ is greater than an isolation threshold $T_I$ for all $j \neq i$. Caglayan[11] has also recognized this distinguishability problem and has suggested a similar approach. We have not attempted to determine an isolation threshold for this study. However, it is clear that an isolation threshold that is large enough to be effective at preventing incorrect isolations will cause a significant delay in the isolation of the failure, perhaps 10 s or more.

Figure 5 shows the GLR detection decision functions for this simulation. (Note the difference in scale from Fig. 3.) In many respects, Fig. 5 resembles Fig. 3. Immediately following the failure, the aileron and flap decision functions increase rapidly. At $t = 12$ s, however, the rate of increase of these decision functions slows, due to the finite data window. To a lesser degree, the elevator and ruddder decision functions increase also. Detection occurs 0.48 s after the failure.

Figure 6 shows the GLR isolation decision functions $DF_{2,3}$, $DF_{2,5}$, and $DF_{2,6}$. (Compare with Fig. 4.) Note that the GLR isolation decision functions are somewhat smaller than the OSGLR isolation decision functions. Once again, this is because the finite data window limits the amount of information that can be accumulated about the failure. Also note that even as late as 7.5 s after the failure, $DF_{2,3}$ is occasionally negative, indicating that the failure is in the left aileron, rather than the right aileron. Even at $t = 26$ s, 16 s after the failure, $DF_{2,3}$ is close to zero. This indicates that it will be difficult to isolate a failure of an aileron using the GLR test with a 2 s data window. Thus, the behavior of the OSGLR test seems to be more robust for this case.

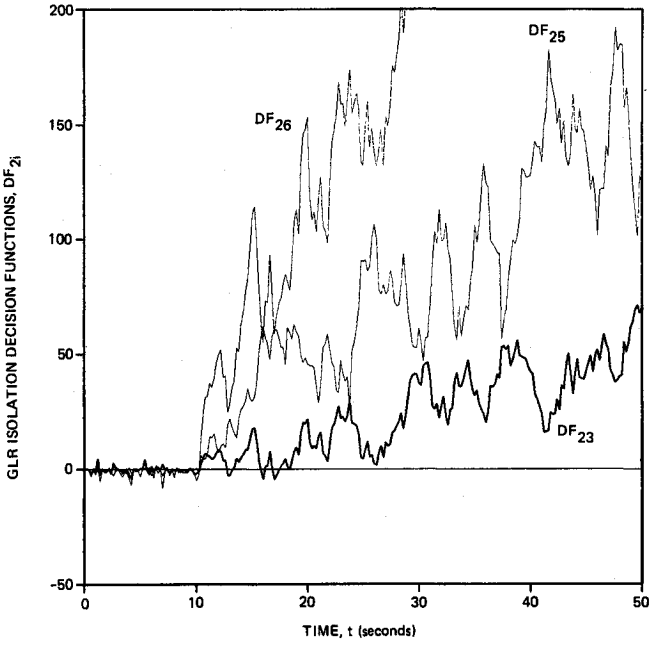


**Fig. 6 GLR isolation decision functions for the linear simulation with a 1 deg bias failure of the right aileron at time $t = 10$ s.**

### Nonlinear Simulation with No Failure

Figure 7 shows the OSGLR and GLR detection decision functions for the nonlinear simulation with no failures. (Only $DF_2$ is shown for each case. $DF_3$, $DF_5$, and $DF_6$ are similar to $DF_2$, and $DF_1$ and $DF_6$ are generally smaller.) Ideally, the OSGLR decision functions should remain well below the detection threshold. However, all the decision functions have peak values that exceed the threshold. For example, the wing control surfaces (corresponding to $DF_2$, $DF_3$, $DF_5$, and $DF_6$) have peak values of approximately 500, which is a factor of 9 larger than the threshold. This effect is due to the differences between the nonlinear model and the linearized model generated from it. It was determined that the greatest source of error is due to mismodeling of the aerodynamic moments about the roll axis. This produces a bias in the estimate of roll rate, which is small compared to the standard deviation of the estimation error. However, this bias is integrated by the Kalman filter to produce a very large bias in the estimate of the bank angle. This, in turn, causes the residual associated with the bank angle measurement to exhibit a significant bias. Because the four wing control surfaces primarily affect the

roll axis, the decision functions assocated with these surfaces are those most affected by this modeling error. The decision function associated with the elevator is also affected, due to coupling between the longitudinal and lateral dynamics.

As was the case with the OSGLR algorithm, the GLR decision functions are larger for the nonlinear simulation than for the linear simulation. In this case, the decision functions corresponding to the control surfaces on the wing reach peak values of approximately 35. This is much lower than the peak values of the OSGLR decision functions. There are two reasons for this. The energy in the residuals due to the biases in the estimation error is correlated over a time period much longer than the length of the data window. Hence, we might expect that a GLR detector with a longer data window would produce much larger decision functions. In fact, a GLR detector with a 5 s data window produces decision functions about twice as large as those shown in Fig. 7.

The other reason that the GLR decision functions are smaller than the OSGLR decision functions is more subtle. Essentially, each GLR or OSGLR detection finds the failure input $f(t)$ that generates a mean process in the residuals that most closely matches the observed residual process. However, the GLR algorithm considers (in this case) only step failures, whereas the OSGLR algorithm considers more general failure modes. Hence, the OSGLR algorithm can find among its hypotheses a failure input time history that matches the observed residuals more closely than does any of the step failures considered by the GLR algorithm. Thus, the same property of the OSGLR algorithm that makes it robust to failure mode uncertainty also makes it more sensitive to modeling errors.

Clearly, the issue of robustness to modeling uncertainty is a serious one. The modeling errors in the preceding example are serious enough to require either a change in the detection threshold or some method of compensating for the error to prevent false alarms. One method for reducing the sensitivity of the OSGLR test to modeling errors has been proposed by Bonnice et al.[6] The approach addresses the first of the two reasons for this sensitivity discussed above, namely, the accumulation of failure information over a long time period. The approach taken there is to age-weight the measurements, so that the Kalman filter and OSGLR detector "forget" old information. This has the effect of reducing the effective length of time over which the OSGLR test collects failure information, without affecting the test's ability to represent arbitrary failure modes. Another approach, which has yet to be investigated, is to age-weight only the OSGLR equations, i.e, age-weight the measurement equation (13b). Yet another approach, if the effect of the modeling error is primarily a bias, is to implement the separated-bias estimation approach[17-22] and use the estimated bias to compensate the residuals prior to the processing by the OSGLR equations. A complete discussion of the issue of sensitivity to modeling errors is beyond the scope of this paper.

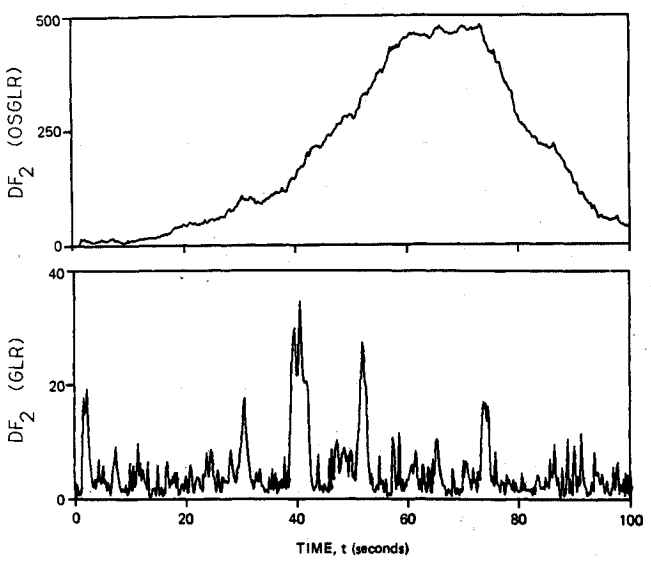


**Fig. 7 OSGLR and GLR detection decision functions for the nonlinear simulation with no failures. Only the decision functions associated with the right aileron are shown; the other decision functions are similar.**

**Stuck Elevator**

In this example, the OSGLR and GLR tests are compared on a test case that is not among the failure hypotheses of either test, namely, a stuck control surface. To generate the example, it was necessary to use the nonlinear simulation of the C-130, with the resulting model error sensitivity problems. For the purposes of this example, the sensitivity problems were avoided by generating the failure early in the simulation, before the effects of the sensitivity are visible. Of course, the sensitivity problem must be addressed in any realistic implementation of the OSGLR test. The example is intended to highlight a specific aspect of the test, specifically its robustness to failure mode uncertainty.

The failure occurred at time $t = 10$ s of a 50 s simulation. Figure 8 shows the resulting error in the elevator position, i.e., the difference between the actual elevator position and the commanded elevator position. Note that the history of the error does not fit into any easily characterized category, such as a bias or ramp failure.

Figure 9 shows the resulting OSGLR detection decision functions. The OSGLR test performs quite well in this case, despite the complexity of the failing input. Approximately 1 s after the onset of the failure, the elevator decision function $DF_1$ increases rapidly, indicating a failure. The other five decision functions also increase, but they are always significantly smaller than $DF_1$. For the threshold selected earlier, the failure is detected at $t = 11.94$ s. (Note, however, that this threshold would not be used unless the problem of modeling errors has been addressed.)

Figure 10 shows the GLR detection decision functions for this case. For the 3 s immediately following the onset of the failure, the GLR decision functions resemble the OSGLR decision functions. (See Fig. 9.) $DF_1$ increases rapidly, indicating a failure of the elevator. For the threshold selected, the detection of the failure occurs at $t = 12.14$ s, 2.14 s after the onset of the failure. This is not significantly different from the OSGLR test.

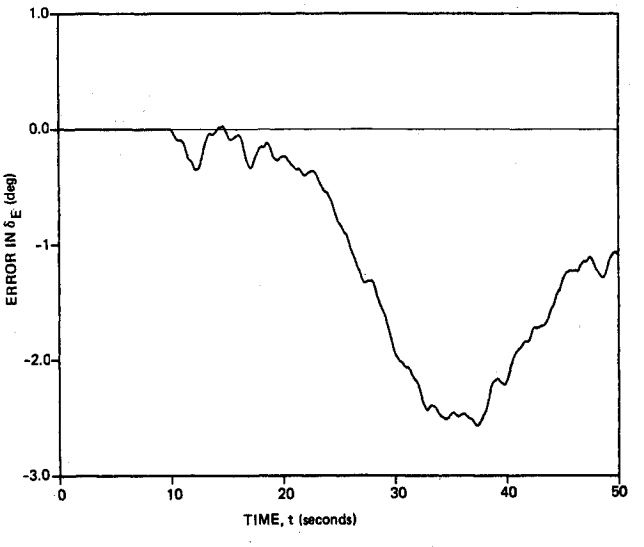


**Fig. 8 Error in elevator deflection due to stuck elevator.**

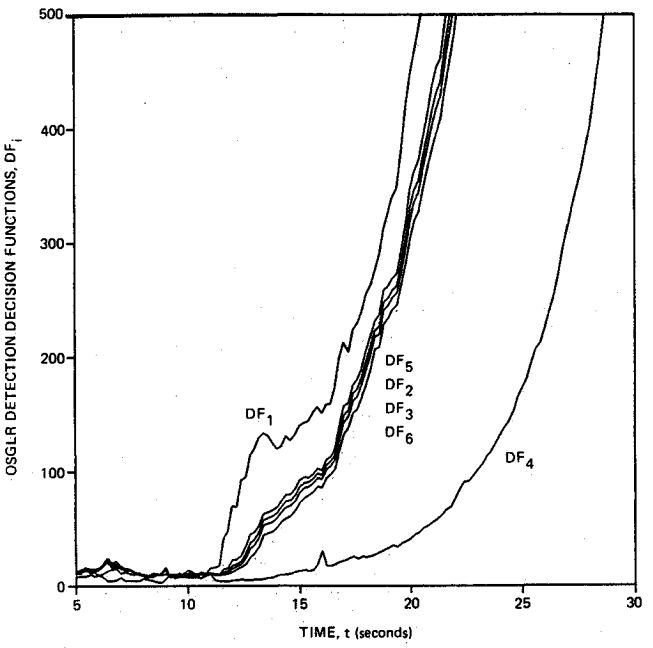


**Fig. 9 OSGLR detection decision functions for the nonlinear simulation with a stuck elevator at time $t = 10$ s.**

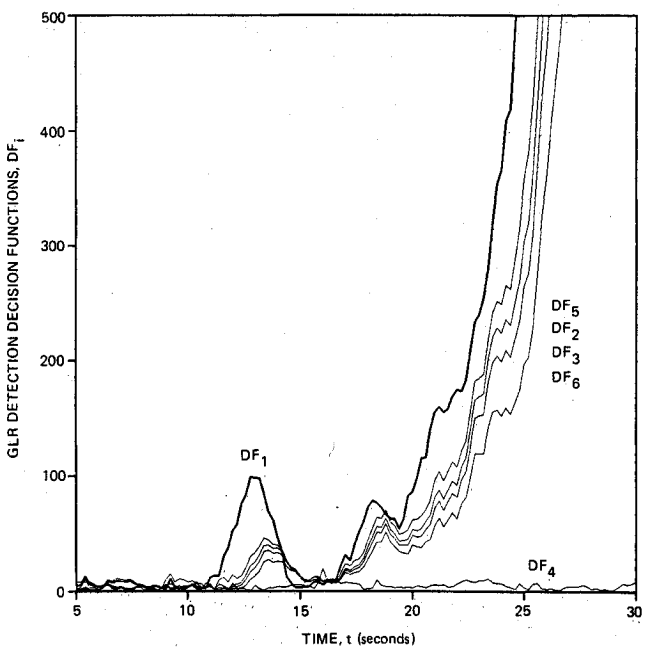


**Fig. 10 GLR detection decision functions for the nonlinear simulation with a stuck elevator at time $t = 10$ s.**

However, this result is somewhat misleading. Note that at about $t = 13$ s, $DF_1$ begins to decrease for the GLR test, until at $t = 15$ s, it is at about the same value that it had before the failure. For a brief time, the four decision functions corresponding to the control surfaces on the wing exceed $DF_1$. At $t = 16$ s, $DF_1$ again increases until $t = 18$ s, where once again $DF_1$ decreases slightly. Shortly thereafter, $DF_1$ begins to increase steadily and is always greater than the other decision functions. Note that if the detection threshold is increased (e.g., to account for modeling errors), then the decision time is likely to increase significantly. For example, if the threshold is set to $T^2 = 200$, then the time of the detection would be $t = 22.52$ s, 12.52 s after the failure. On the other hand, the time to detection for the OSGLR test for this threshold is only 6.82 s.

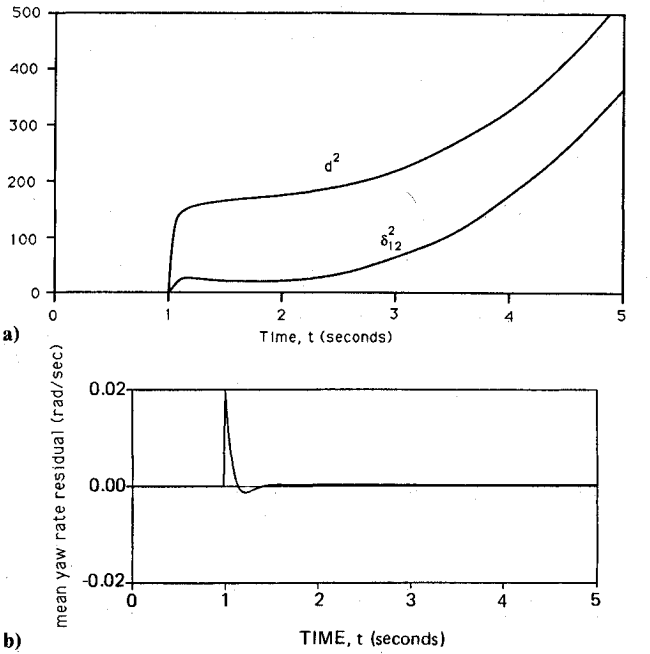


**Fig. 11 Simulation results for a yaw rate gyro bias failure of 0.02 rad/s at $t = 1$ s: a) Noncentrality parameter $\delta^2_{12}$ for the detection decision function $DF_{12}$. b) Mean value of the Kalman filter yaw rate gyro residual.**

This behavior is caused by two separate effects. The first is the relatively short data window. Thus, when the failure input subsides in the vicinity of $t = 15$ s (Fig. 8), the GLR decision function also decreases.

The other reason for this behavior is that the actual failure mode does not agree with any of the hypothesized failure modes of the GLR algorithm. As a result, the results of the test are unpredictable. In particular, $DF_1$ is sometimes less than the other decision functions. Hence, we see that the GLR test is not robust to failure mode uncertainty. Expanding the set of GLR hypotheses to include combinations of ramps and biases can reduce the effect of failure mode uncertainty on the GLR test. However, this is achieved at the price of the substantial computational burden required to estimate the most likely *combination* of onset times for the failure modes assumed. On the other hand, the failure mode can be represented well, or at least approximately, by the OSGLR failure hypotheses. As a result, the OSGLR test is robust to failure mode uncertainty and does not have the undesirable properties of the GLR test displayed in Fig. 10. Furthermore, the OSGLR test does not impose the computational burden that the modified GLR test just discussed would impose.

### Yaw Rate Gyro Bias Failure

In Sec. IV, it was suggested that the OSGLR test may not be well-suited to the problem of detecting sensor failures. To illustrate the difficulties involved, the linear simulation was used to simulate a 0.02 rad/s bias failure of the yaw rate gyro. The bias failure occurs at $t = 1$ s of 5-s simulation.

Figure 11a shows the noncentrality parameter $\delta^2_{12}$ of the yaw rate gyro detection decision function $DF_{12}$. (Recall that the subscript 12 refers to the yaw rate gyro.) It can be shown that

$$E[DF_{12}] = \delta^2_{12} + p \tag{34}$$

where $p$ is the number of basis functions, which in this case is six. The noncentrality parameter is shown rather than the decision function so that the results are not obscured by noise. Also shown in Fig. 11a is the signal-to-noise ratio $d^2$ of the resulting failure signature. Recall that the noncentrality

parameter is bounded by

$$\delta_{12}^2 \leq d^2 \tag{35}$$

where the equality holds only if the failure signature can be represented exactly by the truncated series expansion. In particular, the difference between $d^2$ and $\delta_{12}^2$ shows how much of the energy in the failure signature cannot be represented. In the figure, $d^2$ increases sharply after the failure and then levels off, although it continues to increase at a moderate rate thereafter. On the other hand, $\delta_{12}^2$ is quite small compared to $d^2$ immediately following the failure. At about $t = 1.5$ s, $\delta_{12}^2$ begins to increase moderately. After this time, the difference between $d^2$ and $\delta_{12}^2$ is nearly constant.

This behavior is easily explained. Figure 11b shows the mean value of the Kalman filter yaw rate gyro residual due to the failure. Immediately following the failure, most of the energy in the failure signature is due to this residual. The Kalman filter is a high-pass filter from measurements to residuals. Thus, the step bias failure of the yaw rate gyro produces a spike in the residual that is less than 0.2 s wide. This spike accounts for the large initial jump in the signal-to-noise ratio. As the estimation error is affected by the failed sensor, the other residuals are affected also, although the failure signatures in these residuals are generally smoother. The crux of the problem is that the spike in the residual is not well-represented by the OSGLR failure hypotheses. Roughly speaking, the energy in the residual is concentrated at high frequencies. On the other hand, the other residuals are primarily characterized by low frequencies, so that they are well-represented by the basis functions. Thus, the OSGLR test ignores the spike in the yaw rate gyro residual because it cannot represent it.

Since the failure mode cannot be approximated well using the OSGLR failure hypotheses, the OSGLR test may not be robust to failure mode uncertainty in this case. Specifically, there are two problems. 1) Because $\delta_{12}^2$ is so much smaller than $d^2$, detection may be significantly delayed compared to a test that has a priori knowledge of the failure mode (such as a GLR test designed specifically for the bias failures). 2) It is possible that one of the other decision functions will exhibit a larger response to the failure than $DF_{12}$, so that an incorrect isolation is likely. These problems are not unique to the OSGLR test. Any test, including the GLR test, that depends on knowledge of the failure mode of a sensor will be susceptible to both these problems.

Of these two problems, the first is the most difficult to address. The OSGLR test does not perform as well as the GLR test when attempting to detect sensor bias failure because the GLR test is designed specifically for bias failures. When a bias failure does occur, the GLR test is able to take full advantage of the energy available for failure detection. If we are to improve the OSGLR test's ability to detect bias failures, it is necessary to improve its ability to represent the failure signal in the residual by increasing the number of basis functions used. However, this increases the false-alarm rate and computational burden. Therefore, it is not possible, in general, to deal with the first problem.

The second problem is also difficult to address within the framework of generalized likelihood ratio tests. Two possible approaches are 1) to use direct redundancy instead of analytic redundancy; or 2) to use an FDI algoirthm that is inherently robust to failure mode uncertainty, such as the detection filter of Beard[8] and Jones.[9]

#### Computational Burden

As discussed earlier, the OSGLR test generally requires far less computation than the GLR test. To compare the computational burden of the OSGLR and GLR tests, we measured the CPU time required to implement each algorithm for the example of this paper. The GLR test required 18.5 times more computation than the OSGLR test, for a 2 s data window, with proportionally more computation required for longer data windows. This is not too surprising, given that 100 matched filters must be implemented for each GLR detector (for the 2 s data window).

## VI. Conclusions

In this paper, we have presented a new failure detection and isolation algorithm for linear dynamic systems, the orthogonal series generalized likelihood ratio test. Because of the choice of the failure hypothesis, the test has three desirable features. First, the test is robust to failure mode uncertainty (with a notable exception discussed here), particularly for actuator failures. Second, the test is computationally efficient when compared to other GLR-based tests. This results from the fact that the OSGLR equations are Kalman filter equations in information form. Third, an asymptotic approximation of the false alarm rate of the test, valid for large thresholds, is available in the continuous-time case. Asymptotic approximations of false alarm rate do not exist for most other FDI tests.

However, the OSGLR test may not be well-suited to detecting sensor failures. This is a problem for any FDI test based on Kalman filter residuals, including the GLR test. Finally, the OSGLR test can be very sensitive to modeling errors. It may be possible to reduce this sensitivity somewhat by compensation, but this remains a topic for investigation.

## Acknowledgments

This work was supported by the NASA Langley Research Center under Contract NAS1-17556. Professor Hall was also supported by a fellowship from the Fannie and John Hertz Foundation. The suggestions by three reviewers and the Associate Editor were especially helpful.

## References

[1]Willsky, A. S., "A Survey of Design Methods for Failure Detection in Dynamic Systems," *Automatica*, Vol. 12, No. 6, 1976, pp. 606–611.

[2]Walker, B. K., "Recent Developments in Fault Diagnosis and Accommodation," AIAA Guidance and Control Conference, Gatlinburg, TN, Aug. 1983.

[3]McAulay, R. J., and Denlinger, E., "A Decision-Directed Adaptive Tracker," *IEEE Transactions on Aerospace and Electronic Systems*, Vol. AES-9, No. 2, 1973, pp. 229–236.

[4]Willsky, A. S., and Jones, H. L., "A Generalized Likelihood Ratio Approach to the Detection and Estimation of Jumps in Linear Systems," *IEEE Transactions on Automatic Control*, Vol. AC-21, No. 1, 1976, pp. 108–112.

[5]Lou, X. C., Willsky, A. S., and Verghese, G. C., "Failure Detection with Uncertain Models," *Proceedings of the 1983 American Control Conference*, Inst. of Electrical and Electronics Engineers, Piscataway, NJ, 1983, pp. 956–959.

[6]Bonnice, W. F., Motyka, P., Wagner, E., and Hall, S. R., "Aircraft Control Surface Failure Detection and Isolation Using the OSGLR Test," *Proceedings of the 1986 AIAA Guidance and Control Conference*, AIAA, New York, 1986, pp. 156–164.

[7]Horak, D. T., "Failure Detection in Dynamic Systems with Modeling Errors," *Journal of Guidance, Control, and Dynamics*, Vol. 11, No. 6, 1988, pp. 508–516.

[8]Beard, R. V., "Failure Accommodations in Linear Systems through Self-Reorganization," Ph.D. Thesis, Dept. of Aeronautics and Astronautics, Massachusetts Inst. of Technology, Cambridge, MA, Feb. 1971.

[9]Jones, H. L., "Failure Detection in Linear Systems," Ph.D. Thesis, Dept. of Aeronatuics and Astronautics, Massachusetts Inst. of Technology, Cambridge, MA, Aug. 1973.

[10]Massoumnia, M.-A., "A Geometric Approach to the Synthesis of Failure Detection Filters," *IEEE Transactions on Automatic Control*, Vol. AC-31, No. 9, 1986, pp. 839–846.

[11]Caglayan, A. K., Rahnamai, K., and Allen, S. M., "Detection, Identification and Estimation of Surface Damage/Actuator Failure for High Performance Aircraft," *Proceedings of the 1988 American Control Conference*, Inst. of Electrical and Electronic Engineers, Piscataway, NJ, 1988, pp. 2206–2212.

[12]Motyka, P., Bonnice, W., Hall, S. R., and Wagner, E., "The

Evaluation of Failure Detection and Isolation Algorithms for Restructurable Control," NASA CR-177983, Nov. 1985.

[13]Ostroff, A. J., and Heuschen, R. M., "Investigation of Control Law Reconfiguration to Accommodate a Control Element Failure on a Commerical Aircraft," *Proceedings of the 1984 Automatic Control Conference*, Inst. of Electrical and Electronic Engineers, Piscataway, NJ, 1984, pp. 1746–1754.

[14]Looze, D. P., Krowleski, S. M., Weiss, J. L., Eterno, J. S., and Gully, S. W., "An Approach to Restructurable Control System Design," *Proceedings of the 23rd IEEE Conference on Decision and Control*, Inst. of Electrical and Electronic Engineers, Piscataway, NJ, 1984, pp. 1392–1397.

[15]Hall, S. R., "A Failure Detection Algorithm for Linear Dynamic Systems," Sc.D. Thesis, Dept. of Aeronautics and Astronautics, Massachusetts Inst. of Technology, Cambridge, MA, June 1985.

[16]Van Trees, H. L., *Detection, Estimation, and Modulation Theory*, Part I, Wiley, New York, 1968, Chap. 2.

[17]Friedland, B., "Treatment of Bias in Recursive Filtering," *IEEE Transactions on Automatic Control*, Vol. AC-14, No. 4, 1969, pp. 359–367.

[18]Friedland, B., "Notes on Separate-Bias Estimation," *IEEE Transactions on Automatic Control*, Vol. AC-23, No. 4, 1978, pp. 735–738.

[19]Friedland, B., "Separated-Bias Estimation and Some Applications," *Control and Dynamic Systems*, Vol. 20, edited by C. T. Leondes, Academic, New York, 1983, pp. 1–46.

[20]Caglayan, A. K., "Simultaneous Failure Detection and Isolation in Linear Systems," *Proceedings of the 19th IEEE Conference on Decision and Control*, Inst. of Electrical and Electronics Engineers, Piscataway, NJ, 1980, pp. 1038–1041.

[21]Tacker, E. C., and Lee, C. C., "Linear Filtering in the Presence of Time-Varying Bias," *IEEE Transactions on Automatic Control*, Vol. AC-17, No. 6, 1972, pp. 828, 829.

[22]Ignagni, M. B., "An Alternate Derivation and Extension of Friedland's Two-Stage Kalman Estimator," *IEEE Transactions on Automatic Control*, Vol. AC-26, No. 3, 1981, pp. 746–750.

[23]Chang, C. B., and Dunn, K. P., "On GLR Detection and Estimation of Unexpected Inputs in Linear Discrete Systems," *IEEE Transactions on Automatic Control*, Vol. AC-24, No. 3, 1980, pp. 499–501.

[24]Stratonovich, R. L., *Topics in the Theory of Random Noise*, Vol. 1, Gordon and Breach, New York, 1963.

[25]Blake I. F., and Lindsey, W. C., "Level-Crossing Problems for Random Processes," *IEEE Transactions on Information Theory*, Vol. IT-19, No. 3, 1973, pp. 295–315.

[26]Gelb, A., and Vander Velde, W. E., *Multiple-Input Describing Functions and Nonlinear System Design*, McGraw-Hill, New York, 1968.

[27]Chalk, C. R., et al., *Background Information and User Guide for MIL-F-8785B(ASG), "Military Specification—Flying Qualities of Piloted Airplanes,"* Air Force Flight Dynamics Lab., Wright-Patterson AFB, OH, Tech. Rept. AFFDL-TR-69-72, Aug. 1969.

[28]Lee, Y. W., *Statistical Theory of Communications*, Wiley, New York, 1960, Chap. 18.